RSC Advances

ROYAL SOCIETY OF CHEMISTRY

www.rsc.org/advances

Cite this: DOI: 10.1039/c0xx00000x

www.rsc.org/advances

Article

Fluorescent Diphenylfluorene-pyrenyl Copolymer with Dibenzothiophene-S, S-dioxide and Adamantine Units for Explosive Vapor Detection

Yuerong Wang[a,b], Yixun Gao[a,b], Lei Chen[a,b], Yanyan Fu[a], Defeng Zhu[a], Qingguo He[*a], Huimin Cao[a], Jiangong Cheng[*a], Runsheng Zhang[c], Shuiqing Zheng[c], Songmao Yan[c]

Received (in XXX, XXX) Xth XXXXXXXXX 20XX, Accepted Xth XXXXXXXXX 20XX
DOI: 10.1039/b000000x

Fluorescent diphenylfluorene-pyrenyl Copolymer with dibenzothiophene-S, S-dioxide (**SO**) and adamantine units has been successfully synthesized via Suzuki-Miyaura cross-coupling reaction. After studying the sensing properties of a series of diphenylfluorene-pyrenyl materials to TNT vapor, it indicate that the dibenzothiophene-S, S-dioxide (**SO**) units introduced to diphenylfluorene-pyrenyl copolymers can enhance the photo stability and sensing performance of fluorescent sensing materials simultaneously. This simple strategy can be used as a promising approach for the development of fluorescent conjugated sensing materials.

1. Introduction

The detection of TNT and its analogues, a kind of widely used explosives causing serious security threats and health issues, has been studied for tens of years.[1] Detection of TNT vapor is essential but more challenging because of its low volatility compared to that in solution and solid phases. Therefore, many research efforts now have been put into fluorescent conjugated polymers (FCPs) due to their higher sensitivity among the detection techniques for their "molecular wire" effect.[2-4] However, the FCPs films generally suffer from poor photo stability, π-π stacking induced aggregation in solid state and low permeability to the analytes, which restrict their sensing performance.[5-6] Till now, some strategies have been aroused in molecular design and film morphology tuning to deal with the aggregation and permeability problems. For the molecular structure modification, pentiptycene, hyper-branched, star-like and cross-linked architectures, bulky spacers and non-conjugated side groups have been introduced into polymer chains.[6-10] For example, Nie et al. introduced a 4-[tris-(4-octyloxyphenyl)methyl]phenyl side chain to poly(2, 7-carbazole) and demonstrated that the large and rigid side chains could reduce the interactions between polymer chains in solid state contributing to the sensitivity due to more accessible space for the explosives.[11] Similar findings were also reported by other groups.[12] For the film morphology tuning, spin-coating and dip-coating are most commonly used, and other approaches like electrospinning, self-assembled monolayer, molecular imprinting, and freeze drying were also employed to increase the area-to-volume ratio of sensing films which could help to improve the sensing performance.[13-17] Zhang et al. prepared a series of pyrene-functionalized films via monolayer assembly which was revealed to be sensitive to trace amount of nitroaromatic vapors.[18] And Xie et al. reported a surface molecular self-assembly strategy for molecular imprinting of polymer nanowires and nanotubes, which showed high capacity of binding TNT molecules.[19] Recent study on TNT vapor detection are mainly focused on making conjugated polymers into nanophases or porous phases to create more contacting sites or pathways for TNT molecules. In those cases, to get high sensitivity and satisfactory selectivity is still challenging.[20-23] Therefore, a simple strategy to enhance the sensing performance will be highly preferred.

Dibenzothiophene-S, S-dioxide (**SO**) has recently been employed in the organic photovoltaics (OPVs), organic light-emitting devices (OLEDs) and organic field-effect transistors (OFETs) as electron acceptor owing to its contribution to the spectral stability and fluorescence quantum efficiency improvement.[24-26] The improved spectral stability was attributed to the electron-withdrawing -SO_2- group in **SO** unit in the backbone. And the **SO** unit is also proved to be effective in lowering the LUMO energy level.[27-28] Jie et al. incorporated dibenzothiophene-S, S-dioxide (**SO**) isomer into the poly [9, 9-bis (4-(2-ethylhexyloxy) phenyl)-fluorene- 2, 7-diyl] (PPF) backbone and investigated their electroluminescent properties.[28] With increasing content of **SO** unit in the polymers, the LUMO levels of the copolymers decreased steadily. Besides, the adamantine groups were also introduced into the fluorescent conjugated polymer as side chains to effectively suppress interchain interactions and generate pathways or cavities for the easier diffusion of explosive molecules into the sensing films.[10]

Herein, in this work, a conjugated diphenylfluorene-pyrenyl structure was chosen as the structural skeleton to guarantee that the LUMO level is higher than that of TNT. **SO** units were introduced for photo stability improvement, affinity tuning and interchain interaction control of the conjugated polymers. Bulky

Cite this: DOI: 10.1039/c0xx00000x

www.rsc.org/advances

Article

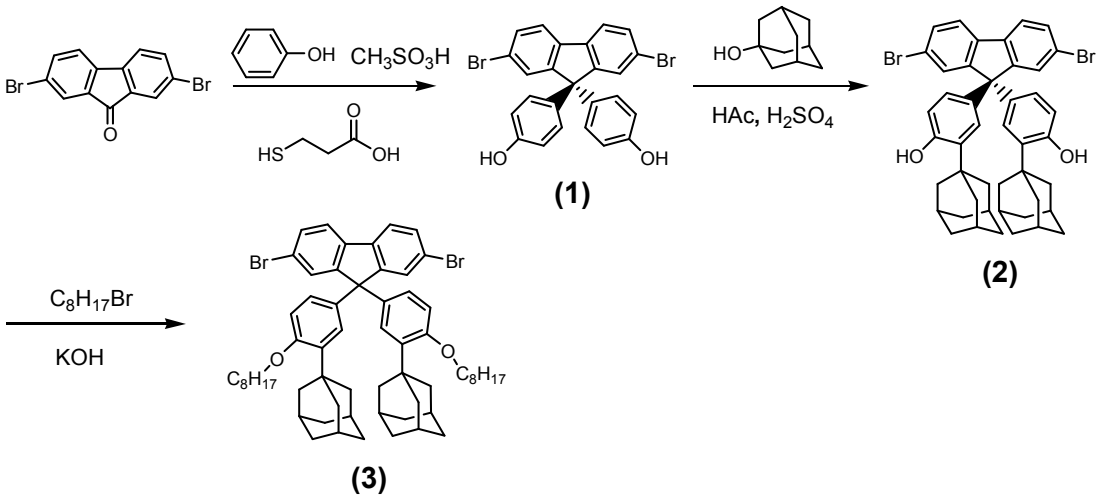

Scheme 1. The synthesis path of fluorene (3).

caged adamantine was employed as pendent units to generate pathways or cavities for the effective diffusion of explosive molecules. Three fluorescent materials, including fluorene-pyrene copolymers without (**P1**) or with (**P2**) **SO** unit and their model compound **M3**, were designed and synthesized. The results of TNT vapor sensing indicated that the introduction of **SO** unit will benefit both photo stability and quenching efficiency of conjugated polymers to TNT vapor. The mechanism of these effects was systematically discussed.

2. Experimental Section

2.1 Instruments

The ^{1}H-NMR spectra were recorded on a Brucker DRX500 instrument, and tetramethylsilane (TMS) was used as an Internal standard. The UV-Vis and fluorescent spectra were obtained from a Jasco UV-760 spectrophotometer and a Jasco FP 6500 spectrometer respectively. The quantum yields of the film were measured with a Jasco FP 6600 Spectrofluorometer with Integrating Sphere and the excitation wavelengths for P1 and P2 are 391 and 373 nm, respectively. Cyclic voltammetry (CV) experiments were performed with a CH Instruments electrochemical analyzer. The electrochemical properties of the materials were investigated by CV with a standard three electrodes (a glassy carbon electrode as a working electrode, a platinum electrode as a counter electrode and a saturated calomel electrode as a reference electrode) electrochemical cell in 0.1 M Bu_4NPF_6 in acetonitrile solution under nitrogen atmosphere with a scanning rate of 100 mV/s at room temperature. Pristine **P1**, **P2** and **M3** films on (10 × 20 mm) quartz plates were spin-coated using 2000 rpm from their solution and placed under vacuum for 30 minutes before use. The fluorescent response of **P1**, **P2** and **M3** films to TNT vapor and other explosives were performed in hermetically-sealed cuvettes at room temperature containing cotton and analytes, and the cotton was on the analytes, which could prevent direct contact between films and analytes and help to maintain a stable vapor pressure. The fluorescent time-course responses were recorded as soon as the quartz plate was exposed to the analyte vapor.

2.2 Synthesis

The synthetic procedures were illustrated in **Scheme 1** and **Scheme 2**. The fluorescent materials **P1**, **P2** and **M3** were synthesized via Suzuki-Miyaura cross-coupling reaction with a yield of 60%, 52% and 86%, respectively. The starting materials including adamantine substituted (2, 7-dibromo-9, 9-bis (4-octyloxy-phenyl)) fluorine (3), 2, 7-bis (4, 4, 5, 5-tetramethyl-1, 3, 2-dioxaborolan-2-yl)-1, 6-dihydropyrene and 3, 7-dibromo-dibenzothiophene-S, S-dioxide (**SO**) were prepared according to the literature [10, 24]. Commercially available reagents were used as received without further purification.

2.2.1 (2, 7-dibromo-9, 9-bis (4-hydroxyphenyl)) fluorene (1)

A 100 mL three-neck flask was filled with phenol (13.160 g, 140 mmol) and 2, 7-dibromofluoren-9-one (4.732 g, 14 mmol). Methanesulfonic (20 mL) and mercaptopropionic (0.075 g, 0.708 mmol) were added to the mixture and then reacted for 16 h at 50ºC. The reaction mixture was then poured into cold water (500 mL). The residue was washed with hot water several times. Petroleum ether was added to the crude products dissolved in ethyl acetate, and then the precipitate was collected and dried in a vacuum oven to provide a light brown solid, monomer **1**. (6.11 g, 86%). ^{1}H-NMR (500 MHz, $CDCl_3$, 25ºC, TMS): δ= 9.41 (s, 2H), 7.89 (d, 2H), 7.55 (d, 2H), 7.47 (s, 2H), 6.87 (d, 4H), 6.65 (d, 4H).

2.2.2 Bisubstituted (2, 7-dibromo-9, 9-bis (4-hydroxyphenyl)) fluorine with adamantine moieties (2)

1-adamantanol (2.736 g, 18 mmol) and monomer **1** (4.572 g, 9 mmol) were dissolved in CH_2Cl_2 (30 mL) at 0ºC, and then a mixture of 98% H_2SO_4 (1.5 mL) and AcOH (7.5 mL) was added

dropwise over 20 min. After 21 h of stirring at room temperature, the resulting mixture was poured into water and extracted with CH_2Cl_2, and the organic phase was dried over sodium sulfate. After the removal of solvent at reduced pressure, the residue was

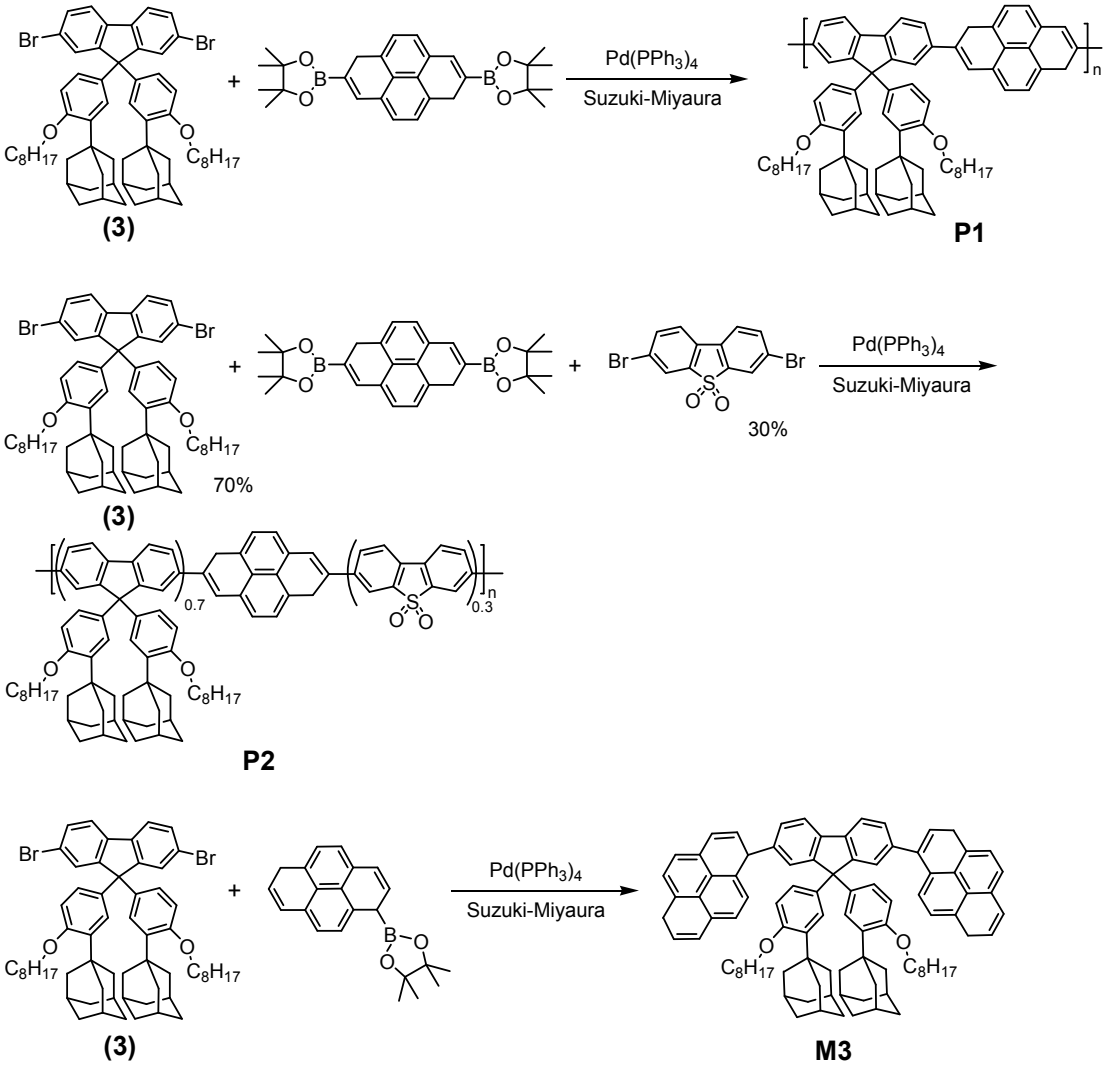

Scheme 2. The synthesis path of **P1**, **P2** and **M3**.

purified by column chromatography on silica gel with ethyl acetate/petroleum ether (v/v=1/6) as an eluent. White solid **2** was obtained by evaporating of the eluent (4.54 g, 65%). In this reaction, **2** may have three ortho-isomers, so **2** in **Scheme 1** was representative of one of the three isomer structures. ^{1}H-NMR (500 MHz, $CDCl_3$, 25ºC, TMS): δ= 7.57 (d, 2H), 7.45 (d, 2H), 7.39 (d, 2H), 7.19 (d, 2H), 6.58 (s, 2H), 6.45 (d, 2H), 4.76 (s, 2H), 2.05 (m, 18H), 1.75 (s, 12H).

2.2.3 Adamantine substituted (2, 7-dibromo-9, 9-bis (4-octyloxyphenyl)) fluorene (3)

Monomer **2** (1.552 g, 2 mmol) and KOH (0.448 g, 8 mmol) were mixed in 25 mL of ethanol. The reaction mixture was heated to 80ºC for 0.5 h, and then 1-bromooctane (1.2 g, 6 mmol) was added dropwise into the reaction mixture. The solution was kept at 80ºC for 20 h. After the reaction was complete, the mixture was poured into water (300 mL), extracted with ethyl acetate and dried over $MgSO_4$. After removal of the organic solvent, the residue was purified by column chromatography on silica gel using ethyl acetate/petroleum ether (v/v=1/15) as an eluent to yield white solid **3** (1.70 g, 85%). ^{1}H-NMR (500 MHz, $CDCl_3$, 25 ºC, TMS): δ= 7.56 (d, 2H), 7.45 (d, 2H), 7.39 (d, 2H), 7.25 (d, 2H), 6.85 (s, 2H), 6.62 (d, 2H), 3.90 (s, 4H), 2.03 (m, 18H), 1.83 (m, 12H), 1.74 (m, 4H), 1.52 (m, 4H), 1.32 (m, 16H), 0.87 (m, 6H).

2.2.4 Poly [(adamantine substituted-9, 9-bis (4-octyloxyphenyl))-pyrenely] P1

A mixture of monomer **3** (300 mg, 0.3 mmol), 2, 7-bis(4, 4, 5, 5-tetramethyl-1, 3, 2-dioxaborolan-2-yl)-1, 6-dihydropyrene (136.8 mg, 0.3 mmol), $Pd(PPh_3)_4$ (44.11 mg, 0.043 mmol), K_2CO_3 (aq, 2 M/10 mL), toluene (20 mL) and ethanol (10 mL) were stirred for 72 h at 85ºC, and the K_2CO_3, toluene and ethanol were charged with nitrogen before adding into the two-neck bottle for a preparation. After cooling to room temperature, the solution was washed with water and CH_2Cl_2, and dried with $MgSO_4$. The organic phase solution was evaporated under reduced pressure to get crude solid product. The crude polymer was then dissolved with least amount of CH_2Cl_2 and precipitated in methanol. The polymer was then further purified by extracting in acetone in a

Soxhlet apparatus for 24 h to remove small molecules impurity, oligomers and catalyst residues. The final product was dried to afford **P1** as a light grey solid (118 mg, 60%). ^{1}H-NMR (500 MHz, $CDCl_3$, 25ºC, TMS): δ= 8.38 (s, 2H), 8.11 (m, 2H), 7.99 (m, 1H), 7.92 (s, 2H), 7.55 (m, 1H), 6.97 (m, 1H), 6.69 (m, 1H), 3.91 (s, 2H), 2.15 (s, 5H), 2.07 (s, 8H), 1.26 (m, 12H), 0.86 (m, 4H). GPC (THF vs. PS): Mn=6241, Mw=14015, PDI=2.24.

2.2.5 Poly [(adamantine substituted-9, 9-bis (4-octyloxyphenyl))-pyrenely-SO] P2

Following the same polymerization procedure as **P1**, with monomer **3** (210 mg, 0.21 mmol, 70%), 2, 7-bis (4, 4, 5, 5-tetramethyl-1, 3, 2-dioxaborolan-2-yl)-1, 6-dihydropyrene (136.8 mg, 0.3 mmol), 3, 7-dibromo-dibenzothiophene-S, S-dioxide (112.2 mg, 0.09 mmol, 30%), $Pd(PPh_3)_4$ (44.11 mg, 0.043 mmol), K_2CO_3 (aq, 2 M/10 mL), toluene (20 mL) and ethanol (10 mL). The final product was dried to afford **P2** as a light grey solid (92 mg, 52%). ^{1}H-NMR (500 MHz, $CDCl_3$, 25ºC, TMS): δ= 8.38 (m, 2H), 8.11 (m, 3H), 7.99 (m, 1H), 7.92 (m, 2H), 7.55 (m, 1H), 6.97 (m, 1H), 6.69 (m, 1H), 3.91 (s, 2H), 2.15 (s, 5H), 2.09 (m, 7H), 1.77 (m, 11H), 1.25 (m, 18H), 0.86 (m, 5). GPC (THF vs. PS): Mn=3850, Mw=4833, PDI=1.25.

2.2.6 Adamantine substituted (2, 7-dipyrenely-9, 9-bis (4-octyloxyphenyl)) fluorene M3

Following the same polymerization procedure as **P1**, with monomer **3** (200 mg, 0.2 mmol), 2-(1, 6-dihydropyren-2-yl)-4, 4, 5, 5-tetramethyl-1, 3, 2-dioxaborolane (132 mg, 0.4 mmol), $Pd(PPh_3)_4$ (44.11 mg, 0.043 mmol), K_2CO_3 (aq, 2 M/10 mL), toluene (20 mL) and ethanol (10 mL). The final product was dried to afford **M3** as a brown solid (215 mg, 86%). ^{1}H-NMR (500 MHz, $CDCl_3$, 25ºC, TMS): δ= 8.23 (m, 2H), 8.21 (m, 1H), 8.19 (m, 1H), 8.14 (m, 1H), 8.10 (s, 2H), 8.02 (m, 4H), 7.99 (m, 1H), 7.68 (m, 2H), 7.32 (m, 1H), 7.00 (m, 1H), 6.68 (m, 1H), 3.91 (m, 2H), 2.27 (s, 1H), 2.01 (s, 1H), 1.95 (s, 4H), 1.80 (m, 3H), 1.65 (m, 8H), 1.53 (m, 4H), 1.25 (m, 15H), 0.85 (m, 6H). ^{13}C-NMR (125.77 MHz, $CDCl_3$) δ =14.07, 22.64, 26.56, 29.09, 29.27, 29.32, 29.58, 29.71, 31.78, 37.13, 37.17, 40.64, 65.15, 67.56, 111.27, 120.09, 124.63, 124.68, 124.97, 125.02, 125.06, 125.39, 125.96, 126.13, 127.34, 127.43, 127.52, 127.83, 128.51, 128.61, 129.87, 130.50, 130.99, 131.51, 137.07, 137.60, 138.15, 138.94, 140.39, 153.47, 156.83 ppm (**Fig S4**). MADLI-TOF MS: m/z=1243.

3. Result and Discussion

3.1 Optical Properties

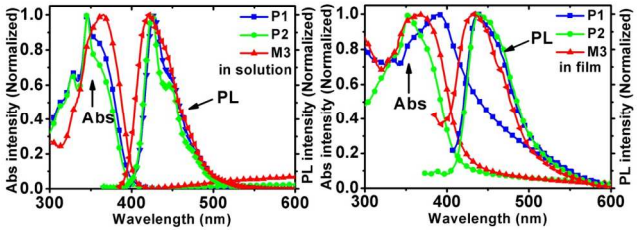

Fig. 1 The UV-Vis. absorption and emission spectra of **P1**, **P2** and **M3** in solution (THF: 10^{-3} M, left) and in films (toluene: 10^{-3} M, right).

The normalized absorption and emission spectra of **P1**, **P2** and **M3** in THF solution and in films are shown in **Fig. 1**. In THF solution, the absorption peaks of **P1**, **P2** and **M3** are at 346, 346 and 365 nm, and the fluorescence emission peaks are at 426, 426 and 421 nm, respectively. The absorption peaks of **P1**, **P2** and **M3** films are at 391, 354 and 369 nm, and the fluorescence emission peaks are at 437, 441 and 433 nm, respectively. In THF solution, **P1**, **P2** and **M3** are highly fluorescent with quantum yields of 0.49, 0.40 and 1 (**Table 1**), respectively.

As is shown in **Fig. 1**, among three materials, **M3** shows the longest absorption peak in THF solution. This could be related to pyrenyl unit since its ratio to fluorene is 2:1 for **M3**, 1:1 for **P1** and 1:0.7 for **P2**.

It could also be seen that, after the incorporation of **SO** unit, the absorption and emission peaks of **P2** in THF solution show little difference from those of **P1**. From solution to film, the absorption and emission peaks of **P2** red-shifted 8 and 15 nm, respectively. However, the absorption and emission peaks of **P1** red-shifted 45 and 11 nm from solution to film, respectively. Furthermore, **P1** film shows a special broad tail peak in its absorption spectrum expanding from 400 to 600 nm which cannot be found in **P2** film. The absorption spectral difference between **P1** and **P2** could be attributed to the fact that there exists a strong interchain π-π stacking interaction in **P1** film but not in **P2** film, which is commonly found in pyrenyl-contained materials because of its large aromatic ring and good excimer-forming capacity. The strong π-π stacking interaction, on one hand, usually results in fluorescence self-quenching, and on the other hand, will provide less contacting sites for analytes and hence lead to a decrease in sensing performance.[29] For further comparison, the quantum yields of P1 and P2 in film were also measured to be 2.24% and 3.14% by a spectrofluometer with integrating sphere. It can be seen that P2 has a larger quantum yield in solid state than that of P1.Thus, the incorporation of **SO** unit helps to prevent the strong π-π stacking interaction in **P2** film.

3.2 Electrochemical Properties

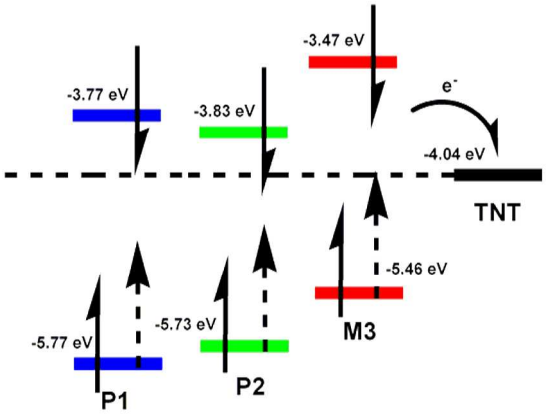

Fig.2 HOMO, LUMO of **P1**, **P2** and **M3** and their PET process to TNT.

According to the photo induced electron transfer (PET) mechanism, to detect TNT vapor, the LUMO level of the sensing probe should be higher than that of TNT to cause the fluorescence quenching process after the excitation (**Fig. 2**). The oxidation and reduction potential of both probes and analytes were obtained via cyclic voltammetry (CV) (**Fig. S1**). The HOMO, LUMO and bandgap data were calculated according to the oxidation and reduction potentials obtained and summarized in **Table 1**.

Since the LUMO levels of **P1** (-3.77 ± 0.020 eV), **P2** (-3.83 ±

0.026 eV) and **M3** (-3.47 ± 0.031 eV) are all higher than that of

Table 1 Optical and electrical properties of **P1**, **P2** and **M3** films.

	Solution (THF)		Film		HOMO	LUMO	ΔE	Φ
	Abs λ_{max} (nm)	PL λ_{max} (nm)	Abs λ_{max} (nm)	PL λ_{max} (nm)	(eV)	(eV)	(eV)	
P1	346	426	391	437	-5.77	-3.77	2.00	0.49
P2	346	426	354	441	-5.73	-3.83	1.90	0.40
M3	365	421	369	433	-5.46	-3.47	1.99	1

[a] Against 9, 10-diphenylanthracene in THF solution (Φ=1, λ_{em}=390 nm)

TNT (-4.04 eV), all the three materials could be theoretically used for TNT sensing basing on PET mechanism (**Fig. 2**). Compared with **M3**, **P1** and **P2** have lower LUMO levels because of the electron delocalization along the conjugated chains. Moreover, **P2** has a relatively lower LUMO level than **P1** owing to the presence of the electron-withdrawing **SO** unit in its backbone.

Therefore, the introduction of **SO** unit could not only decrease the strong π-π stacking interaction between polymer chains in solid state, but also finely tune the energy level.

3.3 Sensing Properties

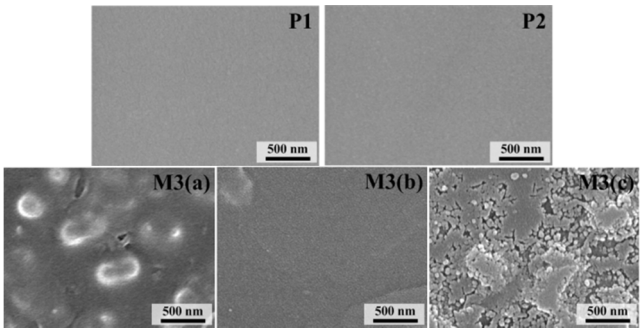

Fig. 3 The surface topography images of **P1** and **P2** films (spin-coated; toluene; 10^{-3} M; 1.0 μm) and **M3** films (spin-coated; 10^{-3} M; (a) toluene; (b) tetrahydrofuran; (c) dichloromethane;) obtained by SEM. All the scale bars are 500 nm.

The relationship of film configuration (for example, the concentration of solution for spin-coating, solvents and film fabrication methods) and sensing properties was studied. The results indicated that solvents and film fabrication methods have little effect on the sensing performance of **P1** and **P2** (**Fig. S2**), while they would greatly affect that of **M3**. Although the π-π stacking interaction in **P1** film is stronger than that of **P2** as indicated from their absorption spectrum, it is inadequate to form agglomerates in **P1** film as that in **M3** film envisioned by SEM (**Fig. 3**). Films fabricated from different concentrations were investigated to optimize the sensing conditions for **P1** and **P2** films (**Fig. 4**). In all cases, **P2** film demonstrates a better sensing performance than **P1** film upon exposure to saturated TNT vapor. And for both **P1** and **P2**, the best concentration of solutions for spin-coating is 10^{-3} M in toluene.

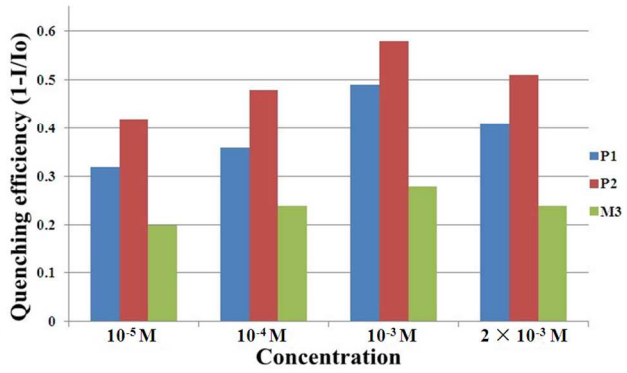

Fig. 4 Quenching efficiencies of **P1**, **P2** and **M3** films in different concentrations (spin-coated; toluene: 10^{-5} M, 10^{-4} M, 10^{-3} M, 2×10^{-3} M) exposed to saturated TNT vapor for 300 s.

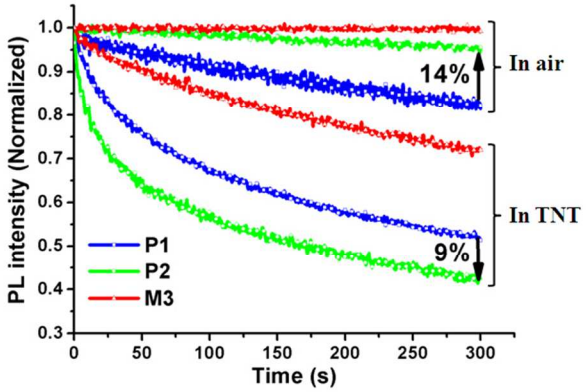

Fig. 5 Sensing properties of **P1**, **P2** and **M3** films (spin-coated; toluene: 10^{-3} M) exposed to saturated TNT vapor and in air in 300 s.

Fig. 5 shows the sensing properties of **P1**, **P2** and **M3** films exposed to saturated TNT vapor (5 ppb) and in air.[30] In neat air, **P2** and **M3** films exhibited excellent photo stability under the excitation of their absorption maxima, but **P1** was relatively unstable (an additional 14% was bleached than that of **P2** film after 300 s exposure). This should be attributed to the electron-withdrawing effect of **SO** unit which reduced the electron density of the backbone and make it more stable to resist the photo oxidation for **P2** film.[28]

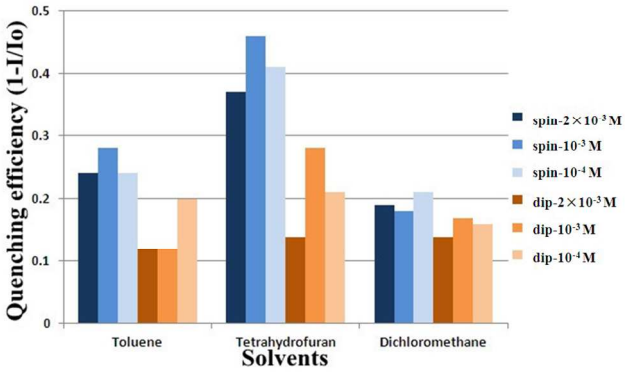

Fig. 6 Quenching efficiencies of **M3** films (Blue: spin-coated; Yellow: dip-coated; (from left to right) solution: toluene, tetrahydrofuran, dichloromethane; concentration: 2×10^{-3} M, 10^{-3} M, 10^{-4} M) exposed to saturated TNT vapor for 300 s.

The emission intensities of **P1**, **P2** and **M3** films were 24%, 36% and 10% quenched respectively after 50 s, and 49%, 58%, and 28% quenched respectively after 300 s upon exposure to saturated TNT vapor. Obviously, **P2** film shows the highest quenching efficiency. Compared to **P1** film, the better sensing performance of **P2** film could be attributed to the incorporation of the electron-withdrawing **SO** unit for two reasons. One reason is that the polar **SO** unit could improve the polarity of polymers thus increasing the affinity between polymers and polar TNT molecules. The other is that **SO** unit could reduce the strong π-π stacking interaction between polymer chains thus providing more contacting sites for analytes. And compared with **P1** and **P2**, small molecule **M3** shows the poorest quenching efficiency which, in one aspect, results from its lack of "molecular wire" effect which usually exists in conjugated polymers leading to an amplified fluorescent signal, and in another, from the serious aggregation of **M3** film (**Fig. 3 (a)**) which gives rise to less contacting sites for TNT molecules. In addition, the fluorescence emission peak positions of **P1**, **P2** and **M3** films show no change after exposure to TNT vapor, indicating a PET mechanism between TNT and the sensing materials. For **M3** film, it was also found that solvents (tetrahydrofuran, toluene, dichloromethane) seriously influenced the sensing property (**Fig. 6**). The highest quenching efficiency of 40% for **M3** film in TNT vapor was achieved from the tetrahydrofuran solution, while the lowest was got from its dichloromethane solution. As is shown in the SEM (**Fig. 3**), the influence of the morphology on the quenching efficiency is caused by the aggregation in different degree. The more serious the aggregation is, the worse the quenching efficiency is. And the optimized sensing property of **M3** film was still worse than that of **P1** and **P2**.

As is discussed above, the affinity between the sensory materials and TNT, the contacting sites in materials for TNT vapor and the "molecular wire" effect in polymers will influence the sensing performance together.

The reversibility of P2 film was checked by a sequential exposure the film to the saturated vapor of TNT (5 ppb) and air for 60 s (**Fig. 7**). It could be found that the quenched sensing films by TNT vapor could be rapidly recovered, and after several cycles, there is only a little attenuation suggesting a good reversibility of P2 film.

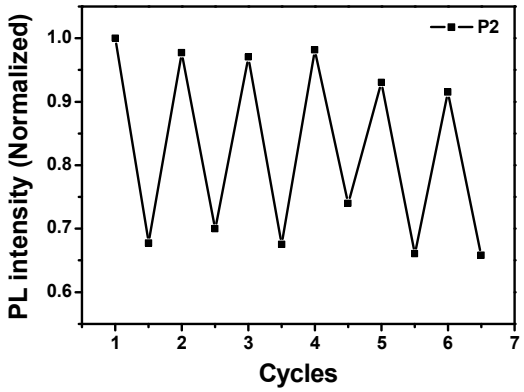

Fig. 7 Cycles of the PL quenching and recovery by exposing the sensing film to the saturated vapor of TNT and air for 60 s sequentially.

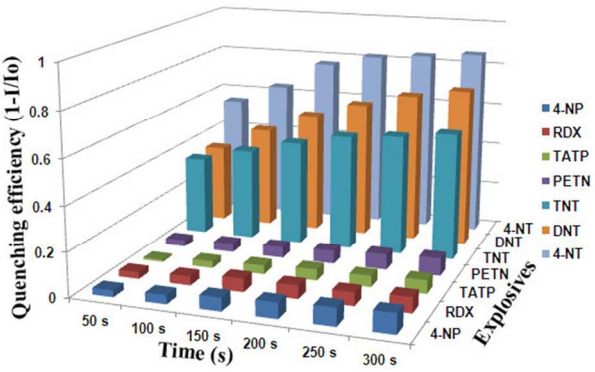

Fig. 8 Quenching efficiencies of **P2** film (spin-coated; toluene: 10^{-3} M) exposed to the saturated vapor of common explosives for 300 s.

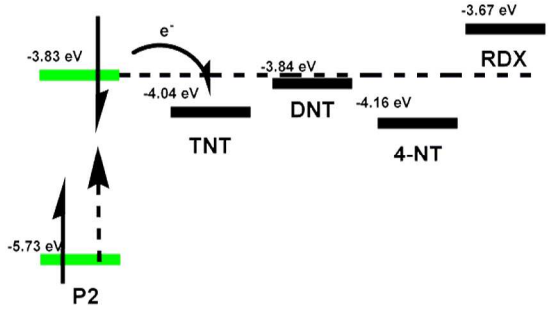

Fig. 9 HOMO, LUMO of TNT, DNT, 4-NT and RDX and the PET process of **P2** to them.

Fig. 8 presents the selectivity of **P2** film to several kinds of explosives. **P2** film shows excellent sensitivity to the saturated vapor of nitroaromatic explosives (NACs) including 4-NT (4-nitrotoluene), DNT (2, 4-dinitrotoluene) and TNT with quenching efficiencies of 86%, 73%, and 58% within 300 s, respectively. However, it is only slightly quenched towards some other explosives like 4-NP (4-nitrophenol), RDX, TATP and PETN. This indicates that the PET process does not occur between **P2** and other explosives which have higher LUMO levels than **P2** like RDX (**Fig. 9**). In contrast, the LUMO levels of NACs (TNT, -4.04 eV; DNT, -3.84 eV; 4-NT, -4.16 eV, calculated from the CV curves as shown in **Fig. S1**) are all lower than that of **P2,** which guarantees the occurring of the PET process.[31]

Furthermore, it is found that their quenching efficiencies to NACs increase with the increasing saturated vapor pressure of NACs from 5 ppb to 215 ppm (TNT, 5 ppb; DNT, 290 ppb; 4-NT, 215 ppm) at room temperature.[30] The results indicate that **P2** film shows satisfactory selectivity toward NACs. Furthermore, the effect of vapors of common solvents on the sensing performance of **P2** film was also checked (**Fig. S3**). It is shown that **P2** film is quite stable or only slightly quenched in the saturated vapor of common solvents including toluene, tetrahydrofuran, dichloromethane, acetic ether, acetone and ethanol.

4. Conclusion

In summary, a simple and effective approach was proposed for nitroaromatic sensing materials by incorporating a dibenzothiophene-S, S–dioxide (**SO**) unit and adamantine units into the diphenylfluorene-pyrenyl backbones. After the incorporation of **SO** unit, the stronger affinity of the sensory materials to TNT and the effectively prevented aggregation for more contacting sites in polymer films for TNT vapor will help to improve the sensing performance of conjugated polymers together. **SO** unit could also be useful in elevating the photo stability of polymers by reducing the electron density in polymer backbones to resist photo oxidation.

Compared with reported results, the simple strategy we used can bring about relatively good sensing performance and satisfactory selectivity for sensory materials to NACs. Further work is still required to achieve higher quenching efficiency and rapid response to TNT vapor. For a much higher sensitivity, one way is a further optimization of the ratio of **SO** of **P2** may increase the interaction force between the sensory material and TNT molecule and hence to increase the sensitivity, another way is to prepare a nano and porous film, which will increase the area to volumn ratio of the sensory film and hence improve the sensitivity, it will be our next goal. This proposed strategy can be used as a promising approach to the development of fluorescent conjugated sensing materials.

Acknowledgements

The authors thank the research programs from the National Natural Science Foundation of China (No. 21273267, 61325001, 61321492 and 51473182), Ministry of Science and Technology of China (Program No. 2012BAK07B03), and Shanghai Science and Technology Committee (Grant No. 11JC1414700).

Notes and references

[a]*State Key Laboratory of Transducer Technology, Shanghai Institute of Microsystem and Information Technology, Chinese Academy of Sciences, 865 Changning Road, Shanghai 200050, China. Fax: 86-21-62511070-8934; Tel: 86-21-62511070-8967; E-mail: hqg@mail.sim.ac.cn (Q. G. He), jgcheng@mail.sim.ac.cn (J. G. Cheng).*

[b]*University of Chinese Academy of Sciences, 19 Yuquan Road, Beijing 100039, China*

[c]*Shanghai Key Laboratory of Crime Scene Evidence, Shanghai Institute of Forensic Science, 803 North ZhongShan No.1 Road, , Shanghai 200083, China.*

† Electronic Supplementary Information (ESI) available: [CV curves and quenching efficiences of P1 and P2 film prepared by different solvent]. See DOI: 10.1039/b000000x/

1 M. Krausa, A. A. Reznev, *Kluwer Academic Publishers: Boston*, 2004.
2 T. M. Swager, *Acc. Chem. Res*, 1998, **31**, 201-207.
3 J. W. Gardner, J. Yinon, Kluwer, *Academic Publishers*, 2003.
4 C. Deng, Q. He, C. He, L. Shi, J. Cheng, T. Long, *J. Phys. Chem. B,* 2010, **114**, 4725-4730.
5 K. Brunner, J. W. Hofstract, *Macromolecules*, 2003, **36**, 500-507.
6 J. S. Yang, T. M Swager, *J. Am. Chem. Soc*, 1998, **120**, 11864-11873.
7 J. Du, Q. Fang, D. Bu, S. Ren, A. Cao, X. Chen, *Macromol. Rapid. Commun*, 2005, **26**, 1651-1656.
8 W. J. Lin, W. C. Chen, W. C. Wu, Y. H. Niu, A. K. Y. Jen, *Macromolecules*, 2004, **37**, 2335-2341.
9 Q. Zhao, W. Wu, *Polymer*, 2009, **50**, 998-1004.
10 H. F. Leng, W. H. Wu, *Reactive & Functional Polymers*, 2012, **72**, 206-211.
11 H. Nie, Y. Zhao, M. Zhang, Y. Ma, M. Baumqarten, K. Müllen, *Chem. Commun*., 2011, **47**, 1234-1236.
12 J. Yang, T. M. Swager, *J. Am. Chem. Soc.*, 1998, **21**, 11864-11873.
13 A. Greiner, J. H. Wendorff, *Angew. Chem. Int. Ed.*, 2007, **46**, 5670-5703.
14 K. Y. Hua, C. M. Deng, C. He, L. Q. Shi, D. F. Zhu, Q. G. He, J. G. Chen, *Chinese Chemical Letters*, 2013, **24**, 643-646.
15 M. J. Shin, M. Yang, J. S. Shin, *Particulate Science and Technology*, 2012, **30**, 543-552.
16 D. Nie, D. J, D. Zhang, Y. Liang, Y. Xue, T. Zhou, L. Jin, G. Shi, *Sensors and Actuators B*, 2011, **156**, 43-49.
17 W. E. Lee, C. J. Oh, I. K. Kang, G. K, *Macromol. Chem. Phys.*, 2010, **211**, 1900-1908.
18 S. Zhang, F. Lu, L. Gao, L. Ding, Y. Fang, Langmuir, 2007, **23**, 1584-1590.
19 C. Xie, Z. Zhang, D. Wang, G. Guan, D. Gao, J. Liu, *Anal. Chem.*, 2006, **78**, 8339-8346.
20 J. L. Novotney, W. R. Dichtel, *ACS. Marro. Lett.*, 2013, **2**, 423-426.
21 H. Nie, Y. Lv, L. Yao, Y. Pan, Y. Zhao, P. Li, G. Sun, Y. Ma, M. Zhang, *Journal of Hazardous Materials*, 2014, **264**, 474-480.
22 Y. Wang, A. La, Y. Ding, Y. Liu, Y. Lei, *Adv. Funct. Mater.*,2012, **22**, 3547-3555.
23 Y. Long, H. Chen, H. Wang, Z. Peng, Y. Yang, G. Zhang, N. Li, F. Liu, J. Pei, *Analytica Chimica Acta.*, 2012, **744**, 82-91.
24 C. Li, M. Liu, N. G. Pschirer, M. Baumgarten, K. Müllen, *Chem. Rev.*, 2010, **110**, 6817-6855.
25 A. C. Grimsdale, K. L. Chan, R. E. Martin, P. G. Jokisz, A. B. Holmes, *Chem. Rev.*, 2009, **109**, 897-1091.
26 S. M. Goetz, C. M. Erlen, H. Grothe, B. Wolf, P. Lugli, G. Scarpa, *Organic Electronics*, 2009, **10**, 573-580.
27 Y. Li, H. Wu, J. Zou, L.Ying, W. Yang, Y. Cao, *Organic Electronics*, 2009, **10**, 901-909.
28 J. Liu, J. Zou, W. Yang, H. Wu, C. Li, B. Zhang, J. Peng, Y. Cao, *Chem. Mater.*, 2008, **20**, 4499-4506.
29 C. He, Q. He, C. Deng, L. Shi, Y. Fu, H. Cao, J. Cheng, *Synthetic Metals*, 2011, **161**, 293-297.
30 K. J. Albert, D. R. Walt, *Anal. Chem.*, 2000, **72**, 1947-1955.
31 H. Sohn, R. M. Calhoun, M. J. Sailor, W. C. Trogler, *Angew. Chem. Int. Ed.*, 2001, **40**, 2104-2105.